2023

Heterogeneous activation of persulfate by macroscopic nitrogen-doped graphene oxide cubes for the degradation of antibiotic contaminants in water

Rajan A. K. Hirani
Edith Cowan University

Abdul H. Asif
Edith Cowan University

Nasir Rafique
Edith Cowan University

Lei Shi

Shu Zhang

See next page for additional authors

10.1016/j.seppur.2023.124110
Hirani, R. A. K., Asif, A. H., Rafique, N., Shi, L., Zhang, S., Saunders, M., & Sun, H. (2023). Heterogeneous activation of persulfate by macroscopic nitrogen-doped graphene oxide cubes for the degradation of antibiotic contaminants in water. *Separation and Purification Technology, 319,* article 124110. https://doi.org/10.1016/j.seppur.2023.124110

Separation and Purification Technology 319 (2023) 124110

Contents lists available at ScienceDirect

Separation and Purification Technology

journal homepage: www.elsevier.com/locate/seppur

Heterogeneous activation of persulfate by macroscopic nitrogen-doped graphene oxide cubes for the degradation of antibiotic contaminants in water

Rajan Arjan Kalyan Hirani [a], Abdul Hannan Asif [a], Nasir Rafique [a], Lei Shi [b], Shu Zhang [b], Martin Saunders [c], Wenjie Tian [d], Shaobin Wang [d], Hongqi Sun [a,*]

[a] School of Science, Edith Cowan University, Joondalup, WA 6027, Australia
[b] College of Materials Science and Engineering, Nanjing Forestry University, 210037 Nanjing, China
[c] Centre for Microscopy, Characterisation and Analysis, The University of Western Australia, Perth, WA 6009, Australia
[d] School of Chemical Engineering and Advanced Materials, The University of Adelaide, Adelaide, SA 5005, Australia

ARTICLE INFO

Keywords:
Graphene cubes
Graphene macrostructures
Metal-free-catalysis
Non-radical pathways
Sulfamethoxazole

ABSTRACT

As a sustainable and green approach, carbocatalysis, a metal-free strategy, has shown exceptional results in advanced oxidation processes (AOPs). Nonetheless, the recovery of these catalysts has been a major shortcoming over the years. Herein, three-dimensional nitrogen-doped graphene macrostructures (3D-NGMs), in the form of macro cubes, were synthesised by a simple cross-linking and thermal annealing procedure, after which they were employed in the activation of peroxydisulfate (PS) for the degradation of sulfamethoxazole (SMX). The catalytic cubes were loaded with different amounts of nitrogen precursor to investigate the role of nitrogen configuration in the sp^2 hybridised carbon network on AOPs. NGC3 cubes with optimum N-loading exhibited outstanding performance for SMX degradation owing to their optimum N/C ratio. Various reaction parameters were studied to optimise the catalytic system. Comprehensive studies on the radical generation were done and illustrated the dominance of the non-radical pathway leading to the proposal of a possible reaction mechanism for SMX. This study not only suggests the role of nitrogen doping on graphene macrostructures but also provides novel insights into macro catalysis to overcome the recovery challenges posed by nano catalysis.

1. Introduction

With the growth of the human population, antibiotics have been used widely as drugs for treating infectious diseases. Common discharge sources of these antibiotics include hospitals, pharmaceutical industries, and wastewater treatment plants [1,2]. Their presence in the discharge after wastewater treatment is a clear indication of their persistent nature to common treatment technologies, classifying them as emerging contaminants (ECs) [3]. One such antibiotic is sulfamethoxazole (SMX), sulfonamide, which is a highly efficient drug used against bacterial infections [4]. Owing to its low concentration in surface water (0.01 to 2.0 μg L^{-1}), SMX has not shown direct side effects or toxicity to human health. However, continued exposure could lead to resistance to its antibacterial potential leading to the emergence of antibiotic-resistant bacteria which could be a threat [5]. It goes without saying that efficient and sustainable detoxification technologies should be exploited to reduce or eradicate the potential risks caused by these antibiotics. Various researchers have studied the degradation of antibiotics such as tetracycline, sulfamethoxazole, amoxicillin, and norfloxacin among others via AOPs [6–8].

Recently, persulfate-based advanced oxidation processes (PS-AOPs) have shown excellent performances in the mitigation of antibiotic pollution owing to their high oxidative potential, low energy input, and higher stability [9]. PS-AOPs are generally characterised by two reaction mechanisms: radical and non-radical pathways. In the radical pathway, persulfate (PS) is activated by catalyst(s) producing various reactive species such as sulfate ($SO_4^{\bullet -}$), hydroxyl (•OH) and superoxide ($O_2^{\bullet -}$). Different from the radical pathway, a non-radical pathway is characterised by the production of singlet oxygen ($^1O_2$) from the surface of the catalysts during the reaction between PS and the catalysts [10]. In both reaction pathways, the catalyst plays a significant role in the activation of PS. Transition metal-based catalysts such as zerovalent iron, iron

* Corresponding author.
E-mail address: h.sun@ecu.edu.au (H. Sun).

https://doi.org/10.1016/j.seppur.2023.124110
Received 27 March 2023; Received in revised form 3 May 2023; Accepted 13 May 2023
Available online 18 May 2023

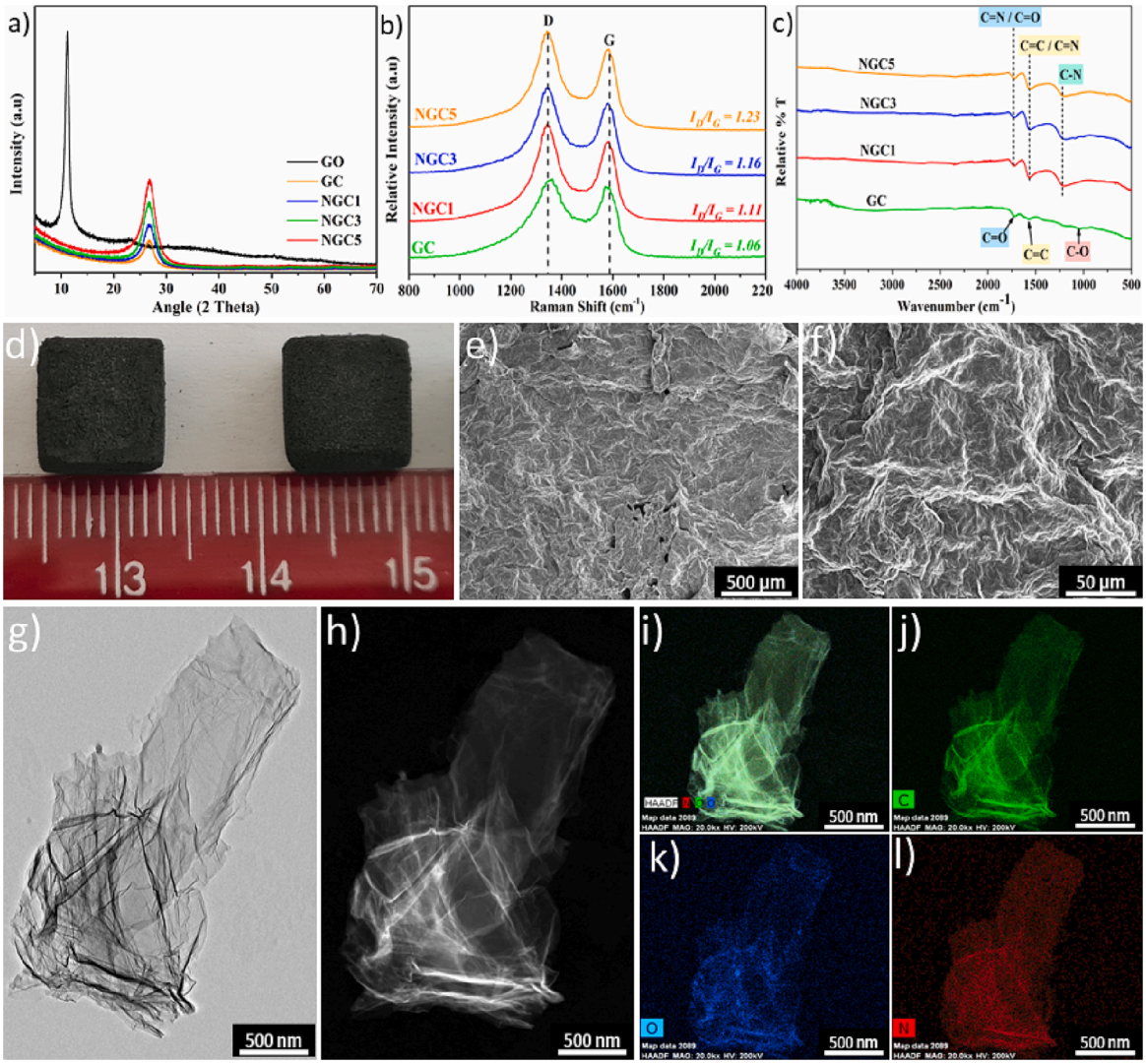

Fig. 1. (a) XRD spectra, (b) Raman spectra of the synthesised cubes, (c) FT-IR spectra, (d) optical photograph of NGC3, (e-f) SEM image of NGC3, (g) TEM image of NGC3, (h) HAADF-STEM image of NGC3 and (i-l) energy dispersive X-ray spectroscopy (EDS) elemental maps of NGC3.

oxide, cobalt oxide, manganese oxide, magnesium oxide, and titanium dioxide among others, have been widely employed for the activation of PS [11–13]. However, these metal-based catalysts suffer from metal leaching causing secondary contamination. In addition, some of these metal oxides are harmful to human health causing additional concerns. Further, metal-based catalysts are pH dependent limiting their application in a wide range of pH. To overcome these challenges, scientists have developed metal-free catalysts based on carbonaceous materials such as nanodiamonds [14], graphene [15], carbon nanotubes [16], and activated carbon materials [17]. With myriads of favourable physiochemical characteristics such as large surface area, reactivity in a wide range of pH, and their abundance on the earth's surface, carbon-based catalysts have satisfactorily overcome the challenges posed by metal-based catalysts. Despite having such fantastic catalytic properties, carbon-based catalysts still have a major challenge in terms of separation and recovery due to their nanoscopic nature [17]. In recent years, three-dimensional (3D) graphene-based materials have sparked a novel approach in catalysis which has significantly helped in overcoming the shortcomings posed by nanocatalysts.

Graphene, a 2-dimensional (2D) sp^2 hybridised carbon structure with various excellent physiochemical properties, has shown its tremendous footprint in AOPs. With superior properties compared to their 2D parent materials, 3D graphene macrostructures (3DGMs) have exhibited a brilliant performance in the adsorption/absorption of oil, dyes, pharmaceuticals, and other organic and inorganic pollutants [18]. The enhanced activity of these 3DGMs could be associated with active components in the 3D interconnected structure which prevents the aggregation of graphene as in 2D structure thus enhancing the mass transfer of the target pollutants. Recently, these 3DGMs have been applied in AOPs in their pure and structurally modified forms. Notably, 3D cobalt oxide-doped graphene aerogels have been used with peroxymonosulfate (PMS) for the removal of Orange II with Co leaching still inevitable [19]. As such, the introduction of metal-free dopants such as N, B, S and/or P could be beneficial in the reduction of secondary pollution as a result of leaching. Previous studies have shown that the incorporation of N into 2D graphene increased its catalytic efficiency without causing any secondary pollution such as metal leaching [20]. A similar strategy could be applied to 3DGMs by co-construction with nitrogen-rich crosslinkers such as urea which could introduce functional groups for improving the catalytic efficiency. In addition, the nitrogen configuration on the carbon skeleton, the surface area, and other various properties could be manipulated by regulating parameters such as GO concentrations, type of N-precursor, amount of N-precursor, and calcination temperature among others [21].

In this study, macro cubic structures were synthesized to overcome the challenges posed by large bulk monoliths synthesised in the past as

they have specific applications in flowing liquids and have also shown positive results in fragmentation due to their fragile nature causing secondary pollution [22]. Herein, 3D N-doped GO cubes were synthesised using a cross-linking technique followed by freeze drying and calcination. In order to deeply understand the role of nitrogen configuration in carbon skeleton on catalysis, the amount of urea (N-precursor) was manipulated keeping other parameters constant. The physicochemical properties and surface chemistry of the as-synthesised cubes were investigated via various characterisation techniques. The cubes were then employed in the activation of PS for the removal of SMX to evaluate the catalytic efficiency and various reaction parameters. The catalytic reaction pathways were analysed by quenching tests and electron paramagnetic resonance (EPR). Total organic carbon (TOC) was used to analyse the mineralisation of the degradation system and finally, the reaction intermediates were determined to propose the possible pathways for SMX degradation.

2. Experimental section

2.1. Chemical and reagents

Natural graphite flakes (325 mesh particle), potassium permanganate ($KMnO_4$, 99%), concentrated sulphuric acid (H_2SO_4, 99.99%), hydrochloric acid (HCl, 37%), urea (99%), potassium persulfate (PS, $K_2S_2O_8$), cetyltrimethylammonium bromide (CTAB, 99%), sulfamethoxazole (SMX), *tert*-butanol (TBA), methanol (CH_4O), ethanol (C_2H_5OH), sodium azide (NaN_3), and hydrogen peroxide (H_2O_2, 30%) were procured from Sigma-Aldrich. Ultrapure water (18.2 MΩ cm, 25 °C) was supplied by the Milli-Q water system throughout the experiment.

2.2. Synthesis of graphene oxide

GO was prepared by oxidation of natural graphite flakes (325 mesh, 99% Carbon basis) via modified Hummers method as discussed in our previous work [23].

2.3. Synthesis of nitrogen-doped graphene oxide cubes

N-doped GO cubes were synthesised by a simple two-step freezing and coagulation process as depicted in **Figure S1**. Typically, 100 mL GO dispersion (1 mg/mL) was prepared by dispersing the as-prepared GO sheets in ultra-pure water followed by ultrasonication for 30 min. An equal amount (1 mL) of GO dispersion was pipetted into 10 mm cubic silicon molds. The molds were then placed in a refrigerator maintained at −25 °C for 12 h until the content was frozen. Subsequently, a 200 mL coagulation bath was prepared by dissolving CTAB (15 mg/mL) and urea (3, 9 and 15 g equivalent to 0.1, 0.3 and 0.5 mol of nitrogen) as a nitrogen precursor. The frozen GO cubes were then de-molded and transferred into the coagulation bath where they were aged for 24 h. The cubes were then freeze-dried for 36 h followed by calcination for 1 h at 800 °C under a continuous flow of N_2 with a heating rate of 5 °C/min. The cubes were labelled as NGC1, NGC3 and NGC5 based on the initial nitrogen content. For comparison, GC was synthesized similarly without the addition of nitrogen precursor.

2.4. Materials characterisation

All the characterisation methods and procedures used to analyse the surface and elemental chemistry of the prepared samples are reported in supplementary information under **Text S1.**

2.5. Catalytic degradation tests

Investigation of the catalytic performance of the synthesised cubes was carried out in a batch reactor. Sulfamethoxazole (SMX), a common antibiotic was chosen as a primary contaminant in this experimental set-up. Detailed experimental procedures for the degradation experiments are described in supplementary information under **Text S2.**

3. Results and discussions

3.1. Characterization of graphene-based cubes

The crystallographic structures of the graphene-based materials were analysed using the XRD patterns as shown in Fig. 1a. A strong peak at $2\theta = 11.2^\circ$ appears in the GO spectrum corresponding to (0 0 2) reflection and interlayer spacing of 0.8 nm. After cubic formation and reduction of GO to GC, a new peak at $2\theta = 27.3^\circ$ emerged while the peak at $2\theta = 11.2^\circ$ disappeared which corresponded to the interlayer spacing of 0.3 nm [9]. The reduction of the interlayer spacing could be attributed to the removal of various functional groups and the restoration of the carbon network. Upon nitrogen doping, the degree of crystallinity increased with the increase in nitrogen loading suggesting successful doping into the graphitic framework [24]. It can also be noted that as the nitrogen loading increases, the peak at $2\theta = 27.3^\circ$ broadens suggesting that increasing the nitrogen amount increases the interlayer spacing as more nitrogen atoms are incorporated into the carbon network, thus increasing the interruptions [23,25].

Raman spectra of the graphene-based cubes are displayed in Fig. 1b. The characteristic D and G bands at 1325 and 1570 cm^{-1} were detected respectively. The G band provides evidence of sp^2 hybridisation while the D band shows the defects on the carbon skeleton [26]. The spectra reveal that NGC1, NGC3 and NGC5 have a relatively higher D band compared to GC as evident in the I_D/I_G ratios. The I_D/I_G ratios of GC, NGC1, NGC3 and NGC5 were calculated as 1.06, 1.11, 1.16 and 1.23 suggesting that an increase in nitrogen doping levels caused structural distortion of the carbon network [27]. Based on these results, it can be concluded that NGC5 had the most structural interruptions due to higher nitrogen loading to the well-ordered sp^2 hybridised carbon structure.

The chemistry of functional groups in N-doped graphene-based catalysts plays a critical role in degradation efficiency. Fig. 1c shows the FT-IR spectra of the synthesised cubes. In the spectral scan of GC, the band stretching of C − O, C = C and C = O was observed at 1040, 1580 and 1750 cm^{-1}, respectively, suggesting the presence of carbonyl and other oxygenated functional groups [28]. Upon nitrogen doping, the C − O bond was eliminated, and a new C − N bond was introduced at 1230 cm^{-1}, while the peaks at 1580 and 1750 cm^{-1} were ascribed to the C = C/C = N and C = O/C = N overlap respectively [29,30].

The external morphological structure of the cubes was analysed by an optical photograph (Fig. 1d) and SEM (Fig. 1**(e-f)**). As seen from the optical image, the catalysts had a cubical shape with an approximate length = width = height = 8 mm and weighed ~ 5 mg (averaged by weighing 1, 5 and 10 cubes). It can be noted that the uncalcined cubed had an approximate length = width = height = 10 mm (equivalent to the mold size) and weighed ~ 25 mg. As evident in the FTIR spectra shown in **Figure S2,** the slight shrinkage in size and loss of weight could be due to the calcination effect leading to the loss of hydroxyl groups, and the decrease of carbonyl groups and C–H moieties [31]. SEM images reveal the wrinkled surface of the prepared cubes with possible stacking of multiple GO layers.

Fig. 1**(g-l)** shows the TEM images and their corresponding elemental maps. The TEM-EDS sample was prepared by finely crushing and grinding the as-prepared cubes. The TEM images further justified the wrinkled nature of the nanosheets. The low contrast of the nanosheets under the electron beam could suggest that a few-layered N-doped reduced graphene oxide was formed [32]. Further, the elemental maps revealed the uniform distribution of N, C and O atoms confirming a well-defined N-doped graphene oxide structure. In addition, the elemental maps shown in **Figure S3** also justify the effect of increasing the N-dopant on the structure as the intensity of the signals increases as the doping level increases.

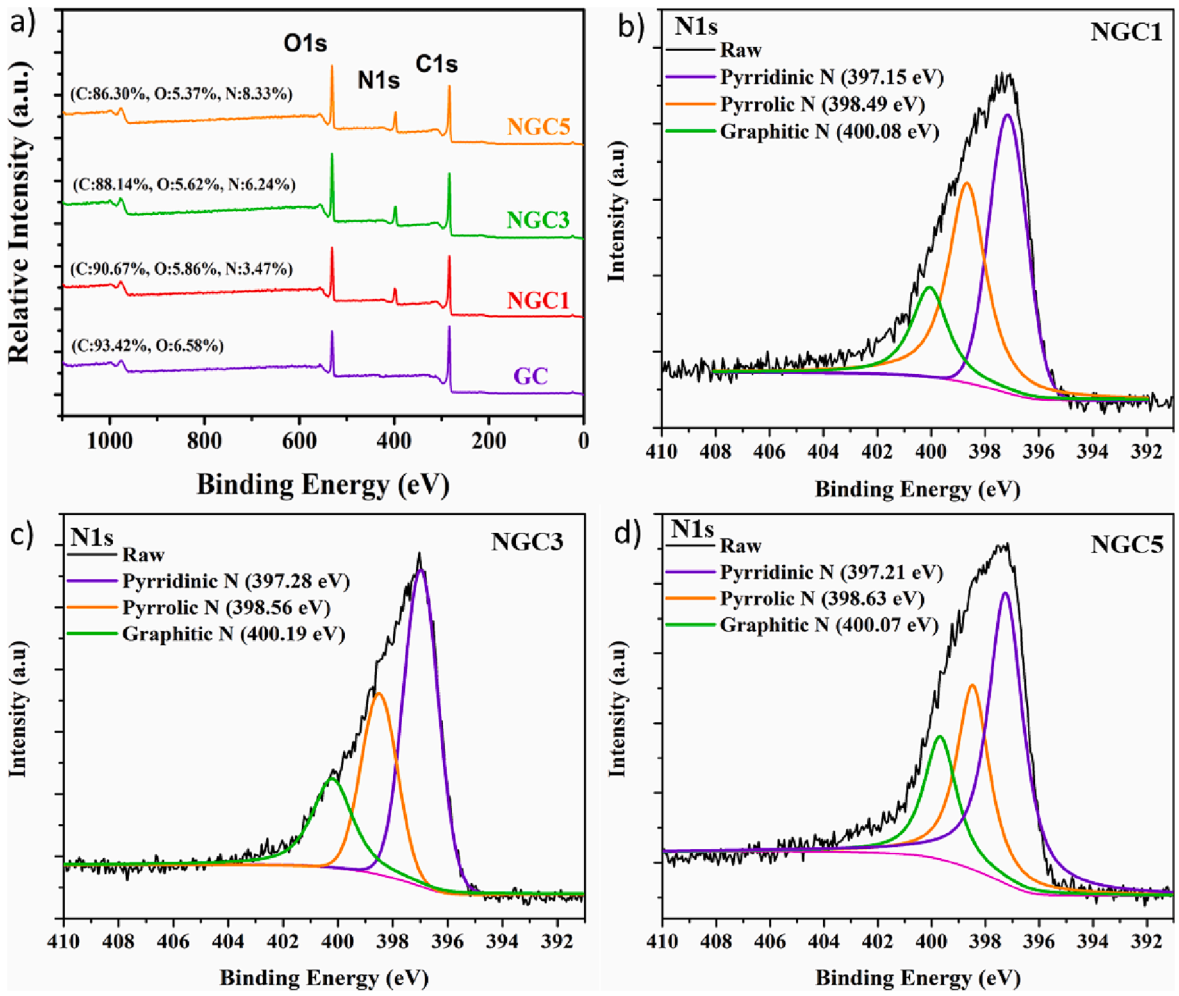

Fig. 2. (a) XPS survey of prepared cubes, high-resolution deconvoluted spectra – N1s; (b) NGC1, (c) NGC3 and (d) NGC5.

Table 1
The N/C atomic ratio, the composition of different types of nitrogen configurations in each catalyst and the BET specific surface area (SSA). N1, N2 and N3 represent pyridinic, pyrrolic and graphitic nitrogen respectively.

Catalyst	N/C (%)	N1 (%)	N2 (%)	N3 (%)	BET SSA (m^2/g)
GC	–	–	–	–	177.8
NGC1	3.83	44.81	36.63	18.56	113.2
NGC3	7.08	43.69	35.21	21.10	76.8
NGC5	9.65	40.72	32.81	26.47	47.9

XPS studies of the synthesised materials were performed to analyse the surface chemistry and the elemental composition. Fig. 2a depicts the survey scan spectra of the graphene-based cubes. The strong characteristic peaks at 283.56 and 531.87 eV representing C and O respectively suggest that high purity samples were synthesised. Further, an additional peak at 398.08 eV in NGC1, NGC3 and NGC5 confirmed that nitrogen was successfully doped on the carbon network. **Figure S4** shows the deconvoluted spectra of C1s for GC, NGC1, NGC3 and NGC5. Three peak fittings of C1s spectra at binding energies ~ 283, 284 and 286 eV corresponded to C − C/C = C, C − O/C − OH and C = N/C = O bonds respectively [33,34]. Additionally, as seen in **Figure S5**, two peak fittings of O1s spectrum at ~ 530 and 531 eV corresponded to C = O and C − O − C/C − OH moieties respectively [34].

The deconvoluted spectra of N1s were also obtained for all N-doped graphene-based cubes (Fig. 2**(b-d)**). The N1s spectra were fitted into three usual peaks binding at ~ 397, 398 and 400 eV ascribing to pyridinic N, pyrrolic N and graphitic N, respectively. The nitrogen doping levels of NGC1, NGC3 and NGC5 were determined to be 3.47%, 6.24% and 8.33% respectively [35,36]. As seen in Table 1, pyridinic N and pyrrolic N decrease while graphitic N increases as the nitrogen precursor increases. This could be attributed to the better stability of graphitic N in the carbon network compared to pyridinic N and pyrrolic N during the doping process [37]. Further, it can be noted that as the nitrogen doping levels are increased, the N/C ratio increases suggesting that the carbon atoms are relatively reduced and are effectively replaced by the nitrogen atoms on the carbon lattice [38].

According to the N_2 adsorption–desorption results (**Figure S6**), the surface area of the prepared catalysts decreased after the N-dopant was introduced. GC showed the highest surface area, which could be due to the expansion and stripping of the graphene layers after the loss of functional groups thus partially restoring the sp^2 hybridised structure [39]. However, as the nitrogen precursor is added the surface area dropped due to the lower exfoliation degree induced by the presence of urea during annealing [40].

3.2. Catalytic degradation of SMX

Sulfamethoxazole (SMX), an antibiotic commonly found in wastewater, was selected as the target pollutant in this study. The removal of SMX via catalytic degradation and adsorption has been depicted in Fig. 3 alongside its respective pseudo-first-order reaction rate constants. Both nitrogen-doped graphene-based cubes and undoped graphene-based

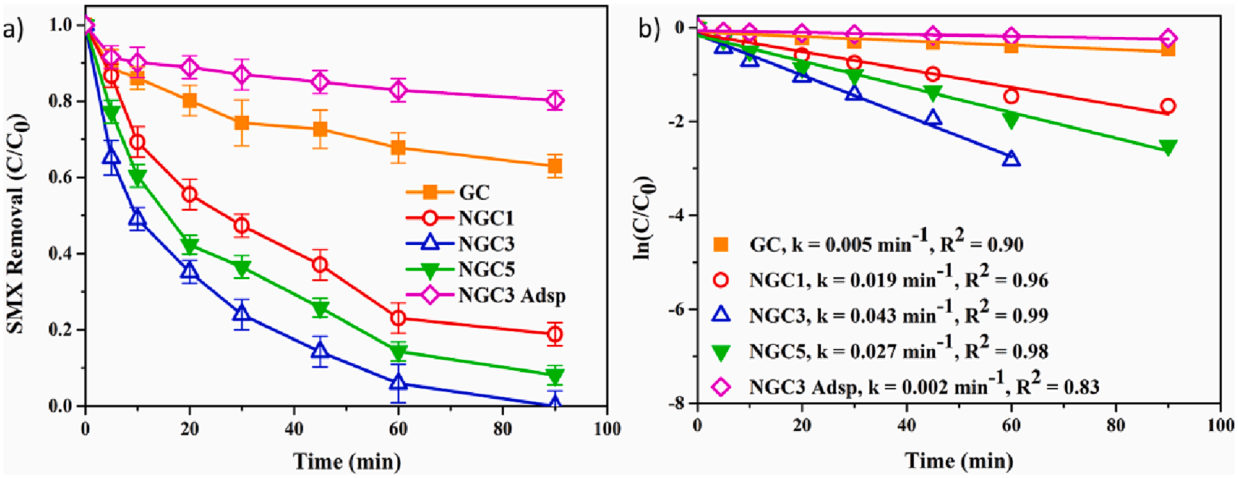

Fig. 3. (a) Preliminary tests for the removal of SMX by the prepared cubes, (b) respective pseudo-first order reaction kinetics fittings. Reaction condition: $[SMX]_0$ = 20 ppm, $[Catalyst]_0$ = 0.2 g/L, $[PS]_0$ = 2.0 g/L and T = 25 °C.

cubes were employed in the catalytic system to monitor the influence of nitrogen loading on the SMX degradation efficiency. It can be seen that the NGC3 system without PS could barely remove any SMX suggesting that adsorption had a negligible role in SMX removal in NGC3/PS system. The SMX adsorption on various cubes has also been presented in **Figure S7**.

It was further noted that GC, undoped graphene cubes, could hardly degrade SMX in 90 min as only 36% SMX removal was recorded. In contrast, when nitrogen was loaded into the graphene-based cubes, the SMX degradation efficiency escalated to 81%, 100% and 92% on NGC1, NGC3 and NGC5 respectively suggesting that the nitrogen loading played a vital role in the activation of PS and consequently degrading SMX. It was worthwhile noting that when the nitrogen level increased from 0 to 0.3 mol, the SMX removal efficiency increased simultaneously which could be attributed to the development of N functional groups [9]. In addition, as the nitrogen level increased, the amount of graphitic N also increased which can effectively break the inertness of the $\pi - \pi$ carbon bonds in the graphene network thus explaining the increased degradation efficiency [37]. Interestingly, it was worth noting that a further increase in nitrogen loading from 0.3 to 0.5 mol led to a decrease in the catalytic efficiency despite having the highest nitrogen loading amount. This suggested that the N loading amount on the graphene-based cubes was not the only factor, and the nitrogen/carbon (N/C) ratio also played a vital role in the catalytic efficiency. Ideally, if more nitrogen atoms are introduced into the carbon network, the amount of positively charged carbons would increase resulting in a better performance in PS activation. However, practically, once excessive nitrogen atoms are introduced, the number of carbon atoms would be relatively decreased thus reducing the active sites. To be more specific, NGC5 had the highest N doping level (8.33%) but the lowest C content (N/C = 9.65%) while NGC1 had the lowest N doping level (3.47%) but had the highest C content (N/C = 3.83%). Despite these differences, NGC3 with an optimal N doping level of 6.24% and an optimal N/C ratio of 7.08% had the best catalytic efficiency suggesting that an appropriate ratio of both N doping level and N/C ratio are necessary. Further, as the N doping levels increased, the SSA oppositely reduced strongly suggesting that nitrogen doping had a dominant role in the SMX degradation [37]. Overall, the synergistic interaction between rGO with high SSA and nitrogen, an electron mediator aiding in efficient electron transfer, would lead to the improved performance of the as-synthesized catalytic cubes in the study.

3.2.1. *Influence of primary reaction parameters*

The catalyst dosage varied between 0.1 and 0.4 g/L and the subsequent results are shown in Fig. 4**(a-b)**. It was noted that the increase in initial catalyst dosage enhanced the removal efficiency. SMX increased, resulting in the increased reaction rate constants (0.021 – 0.056 min^{-1}). The increase in the degradation efficiency could be associated with the increased number of exposed active sites favouring the electron transfer on the surface of the catalyst for the generation of active species.

The effect of the reactive species on the SMX removal efficiency was studied by varying the initial PS dosage. Fig. 4**(c-d)** depicts that as the PS loading increases from 1.0 to 4.0 g/l, the reaction rate constants elevate from 0.022 to 0.066 min^{-1}. This trend could be associated with the increased diffusion of PS on the surface of the catalyst accelerating the generation of more radicals hence increasing the degradation efficiency.

pH plays an important role in the oxidation efficiency as it results in the formation of new radicals which directly affect the oxidation. Fig. 4 **(e-f)** depicts the effect of pH on the SMX degradation efficiency and its adjacent reaction rate constants. It can be seen that degradation efficiency is quite stable at a wide pH range, indicating its feasibility without many limitations of pH modifications. However, it can be seen that when the pH of the solution is highly alkaline, the degradation rate constant drops to 0.015 min^{-1}. The suppression in the degradation efficiency at elevated pH could be attributed to the formation of OH^- which would be adsorbed on the catalytic surface hindering the interactions between PS, SMX and the catalyst [41]. Alternatively, CO_2 produced as the final product from the SMX oxidation could potentially be converted to carbonate and bicarbonate ions under highly alkaline conditions inhibiting SMX degradation [42].

Figure S8**(a-b)** depicts the influence of initial SMX concentration on the catalytic efficiency and their respective pseudo-first-order reaction kinetics. The initial concentration varied from 10 to 40 ppm and the results show that as the SMX concentration increases, the degradation reaction rates decrease from 0.077 to 0.016 min^{-1}. This effect is due to the limited catalytic surface and reactive radicals availability in the solution. Considering all the other factors are constant, the number of active radicals produced remains constant in all four reactions. Thus, increased SMX concentration would need more catalyst loading and/or PS to achieve a better degradation efficiency [43]. To investigate the versatility of the synthesised NGC3, various emerging pollutants were employed in the catalytic system. **Figure S9** shows the degradation efficiencies of phenol, 4- hydroxybenzoic acid (HBA), sulfachloropyridazine (SCP) and trimethoprim (TMP) and their respective reaction rate constants. It can be noted that 100% degradation of phenol and HBA was achieved in 60 min, 100% degradation of SMX and SCP in 90 min and 94% degradation of TMP in 90 min. The above results indicate that NGC3/PS system can degrade a wide range of emerging organic contaminants.

Figure S10 shows the effect of various anions and natural humic acid

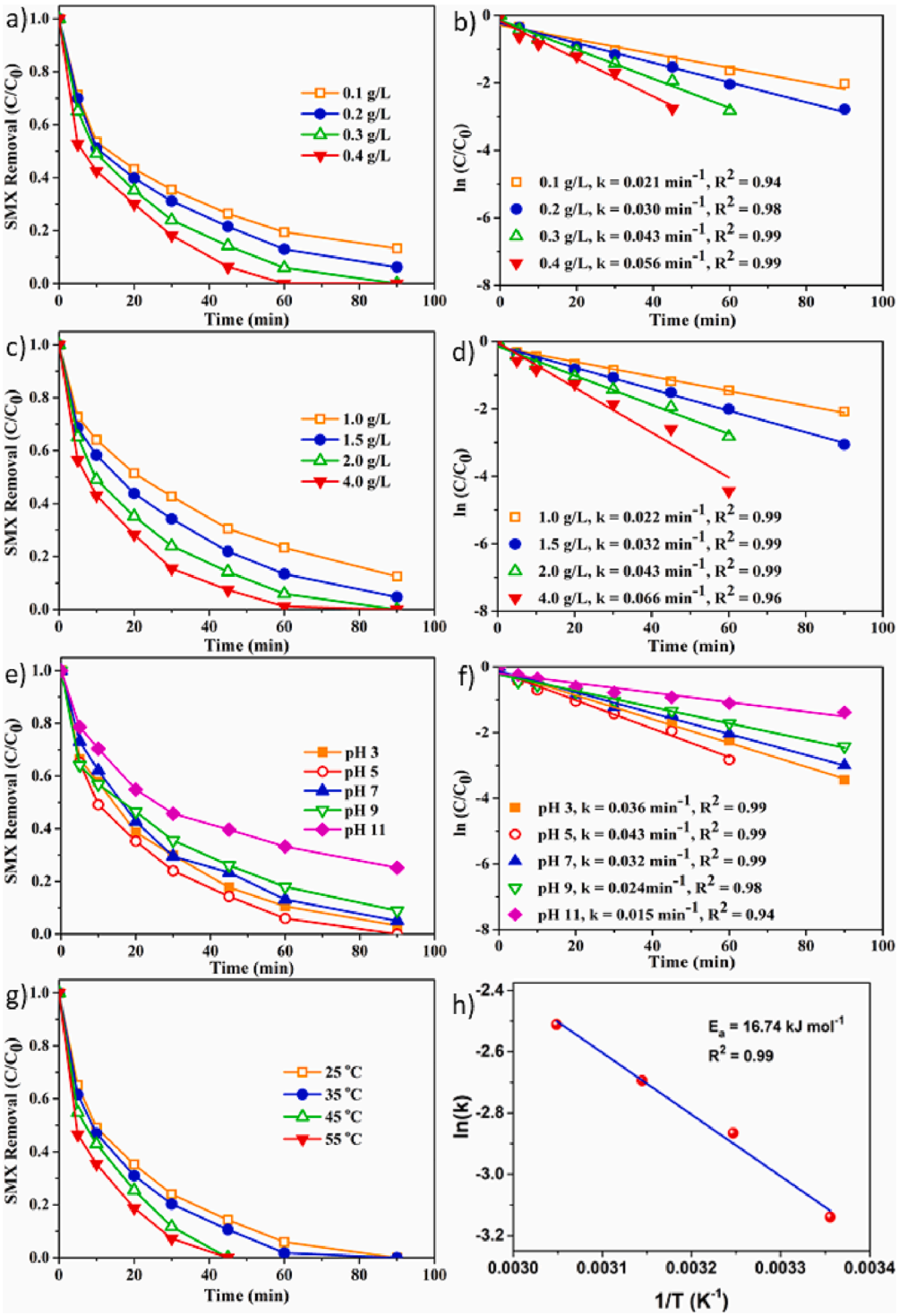

Fig. 4. Effect of various reaction parameters on SMX degradation efficiency: (a) initial catalysts dosage, (c) initial PS loading, (e) initial pH, (g) reaction temperature, (b), (d) and (f) respective first-order reaction kinetics, and (h) calculation of activation energy.

on SMX degradation by NGC3. It was noted that chloride, nitrate, and phosphate ions had a negligible effect on SMX degradation which was in line with previous studies [44,45]. However, when bicarbonate ions were introduced into the reaction system, the reaction rate constant dropped to 0.012 min^{-1}. This could be attributed to the reaction of bicarbonate ions and hydroxyl radical forming HCO_3• which has a lower reaction rate with organic pollutants thus lowering the degradation of SMX [45]. Further, when naturally occurring organic humic acid (HA) was introduced into the SMX degradation system, the reaction rate constant dropped to 0.021 min^{-1} indicating a significant effect on SMX removal. This phenomenon could be a result of the radical scavenging effect. HA is capable of scavenging the reactive species in the system owing to the high oxidation ability of the active radicals [46].

3.2.2. *Catalyst reusability and stability*

The reusability tests were run to investigate the stability of the catalysts after multiple runs. For real-time applications, the stability and reusability of the catalysts are important factors to consider. As such, the

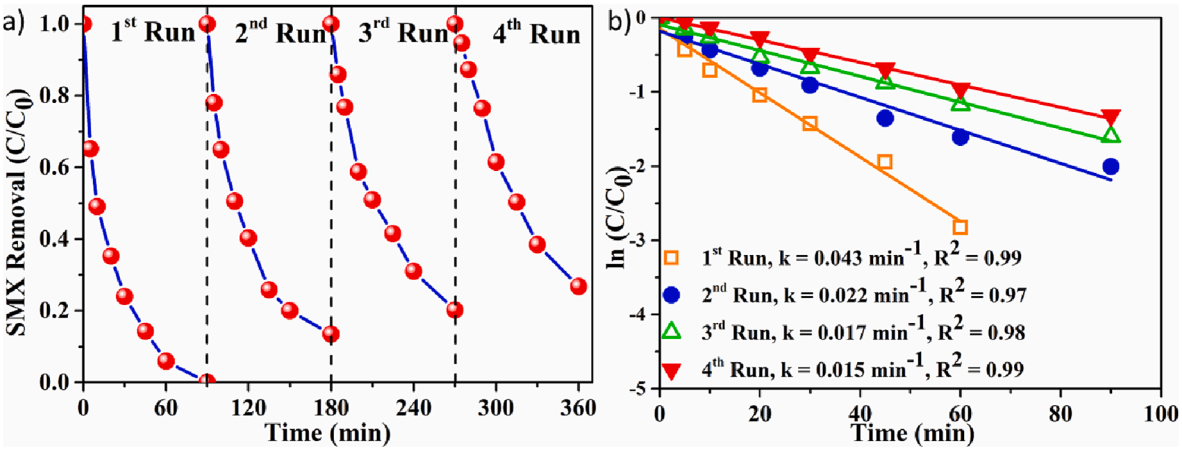

Fig. 5. (a) Reusability tests, and (b) respective first-order reaction kinetics. Reaction condition: $[SMX]_0$ = 20 ppm, $[Catalyst]_0$ = 0.2 g/L, $[PS]_0$ = 2.0 g/L and T = 25 °C.

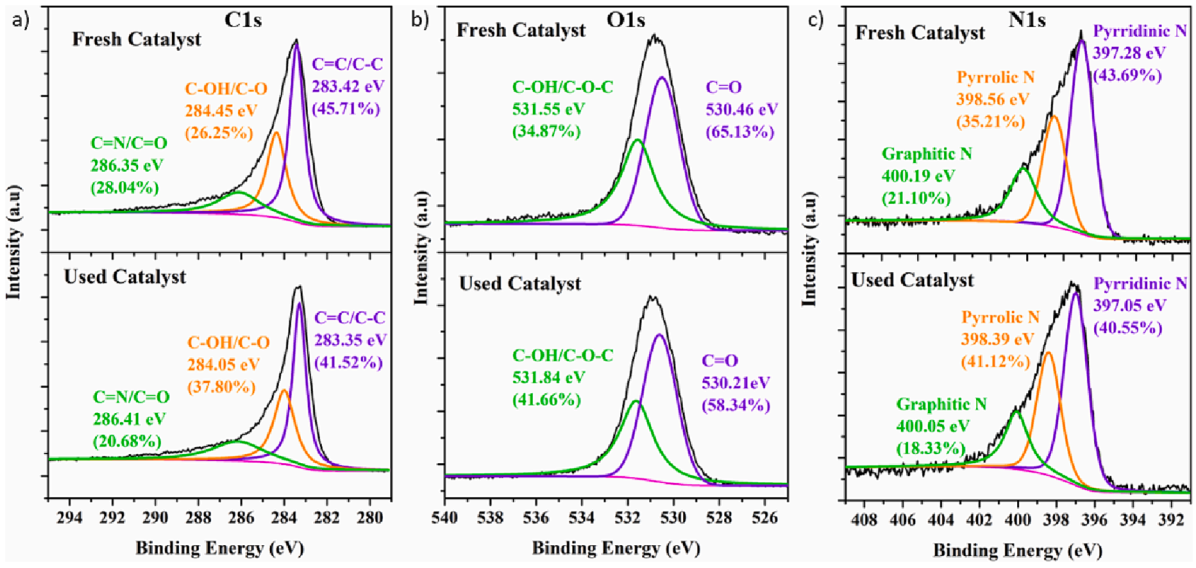

Fig. 6. XPS analysis of fresh and used catalysts; (a) C1s, (b) O1s and (c) N1s.

stability of the NGC3 catalyst was evaluated by four consecutive degradation runs as shown in Fig. 5. After each run, the catalytic cubes were recovered by simply decanting the solution and placed in ultrapure water for dialysis for 6 h. The dialysis water was replaced every 1 h. Thereafter, the cubes were dried at 60 °C overnight. After the first run, a 13% efficiency loss was registered 23% drop in the efficiency was noted after the fourth run suggesting that NGC3 is a highly stable catalyst. The slight decrease in the efficiency could be a result of the residual and intermediate occupation on the active sites. FTIR spectroscopy was further used to determine the effect of degradation on the element bonds and functional groups. As seen in **Figure S11**, a slight change in the used NGC3 spectrum was seen, indicating that well-established coordination between C, N, O and H has increased the stability.

Further, XPS analysis on the used and fresh catalyst was performed to analyse the changes in the chemical bonds and identify the active sites of NGC3 in catalysis. The basis of PS ($O_3SO - OSO_3$) activation is the weakening and the cleavage of superoxide O − O bond and facilitate the transfer of electrons between the catalyst and PS. The high-resolution deconvoluted spectra of C1s and O1s in Fig. 6**(a-b)** depict the versatility of oxygen functional groups on the NGC3 before and after SMX degradation. There were three fitted peaks in C1s centering at ~ 283.42, ~284.45 and ~ 286.35 eV referring to C − C/C = C, C − O/C − OH, and C = O/C = N respectively and two fitted peaks in O1s at ~ 530.46 and ~ 531.55 eV representing C = O and C − O − C/C − OH moieties respectively. It can be noted that from both C1s and O1s spectra, the content proportion of the C = O (ketonic group) and C − O/C − O − C/C − OH changes simultaneously and opposingly indicating the conversion of C = O (ketonic group) to C-OH/C − O/C − O − C moieties in the heterogeneous catalysis. From the above phenomena, it can be implied that the ketonic group (C = O) acts as the Lewis basic site with the lone pair of electrons thus increasing the electron density of the neighbouring carbon atoms in the sp^2 hybridization and promoting its reactivity [47].

The high-resolution spectra of N1s for both fresh and used NGC3 catalysts (Fig. 6c) depict a clear reconstruction of the N bond configuration on the graphene network. It can be noted that the content proportion of pyridinic N and graphitic N decreased from 43.69% to 40.55% and 21.10% to 18.33% respectively while pyrrolic N increased from 35.21% to 41.12% indicating that the nitrogen doping on the hexagonal rings acts as potential active sites and is responsible for initiating the electron flow between NGC and PS [38]. Further, graphitic N has the highest potential to accelerate the electron transfer from one neighbouring carbon atom to another thus breaking the inertness of the π- π conjugated carbon network. This electron transfer results in an increased positive charge of carbon atoms thus weakening the

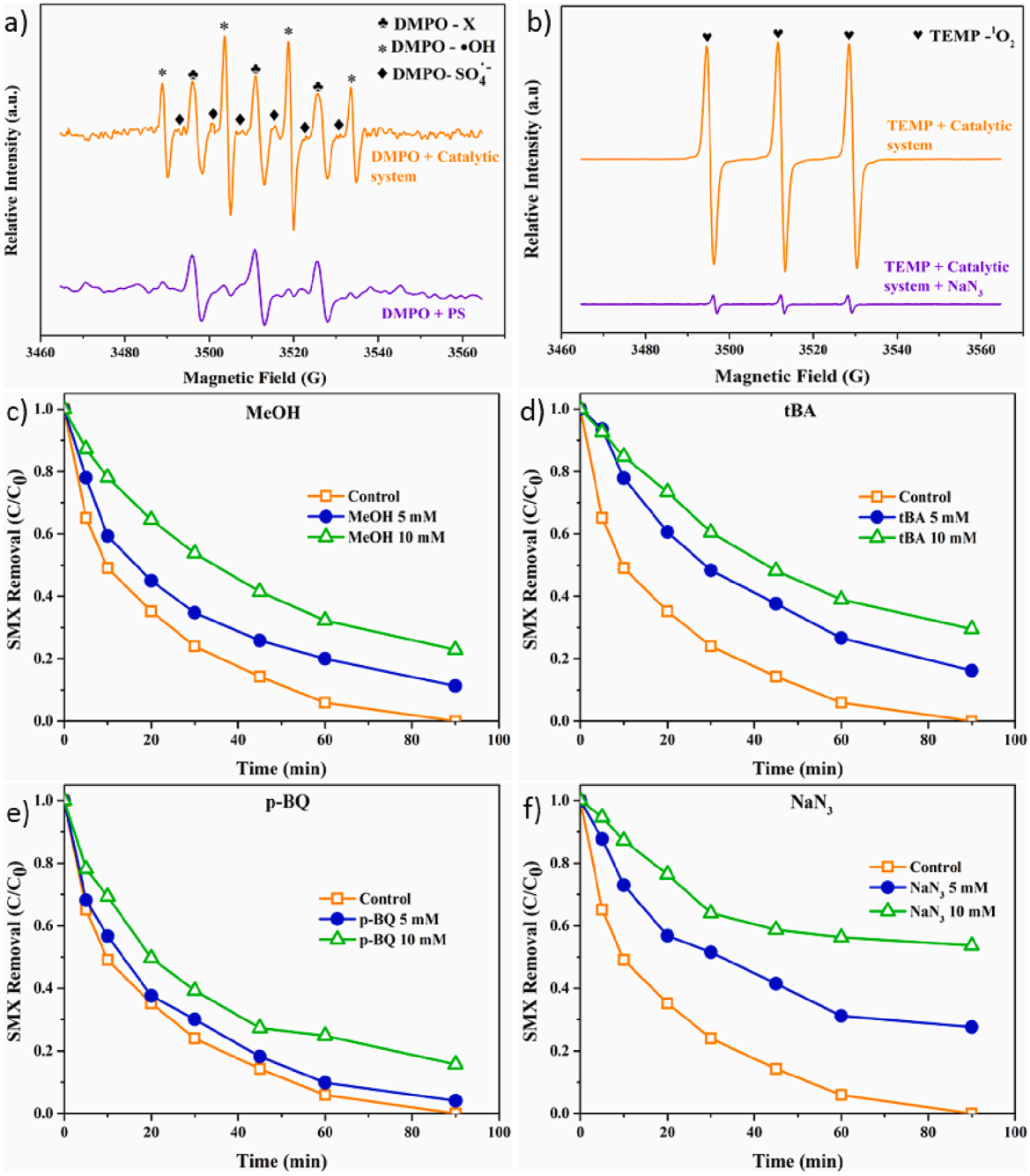

Fig. 7. EPR spectra; (a) DMPO−•OH and DMPO − $SO_4^{\bullet-}$, and (b) TEMP–$^1O_2$, quenching effect on SMX degradation efficiency, (c) MeOH, (d) tBA, (e) p − BQ and (f) NaN_3. Reaction condition: $[SMX]_0$ = 20 ppm, $[Catalyst]_0$ = 0.2 g/L, $[PS]_0$ = 2.0 g/L and T = 25 °C.

negatively charged peroxide O − O bond in PS generating active species ($^1O_2$) via nucleophilic addition reaction of PS with the positively charged carbon atom [38].

From the above arguments, it can be concluded that the slight decrease in the degradation efficiency after the fourth run could be a result of the irreversible conversion of active sites due to cannibalistic surface oxidation or blockage by intermediates [48]. Nonetheless, the high stability of the catalysts could be a result of the dominant role of the non-radical mechanism in alleviating and reducing surface inactivation [9]. Additionally, as compared to the nanocatalysts, it can be noted that the recovery of the macro cubes is much more efficient as simple decantation can be used for collection of the reacted catalysts, unlike nanocatalysts which require techniques such as vacuum filtration, sedimentation, evaporation among others. Further, unlike other bulk graphene macrostructures, no fragmentation was noted while using macro cubes suggesting their feasibility for commercial applications in wastewater remediation processes [22,23].

3.2.3. *Identification of active species and development of degradation mechanism*

PS is known to be activated via radical and/or non-radical pathways. To fully identify the reaction pathway, the identification of reactive species is crucial. Herein, the presence of the active species in the NGC3/PS system was determined by the EPR technique. As shown in Fig. 7a, DMPO was used to capture the $SO_4^{\bullet-}$ and •OH radicals. It was noted that strong peaks of DMPO−•OH and small peaks of DMPO − $SO_4^{\bullet-}$ were recorded in the EPR spectrograph indicating that both $SO_4^{\bullet-}$ and •OH radicals were present in the catalytic system. Further, as seen in Fig. 7b,

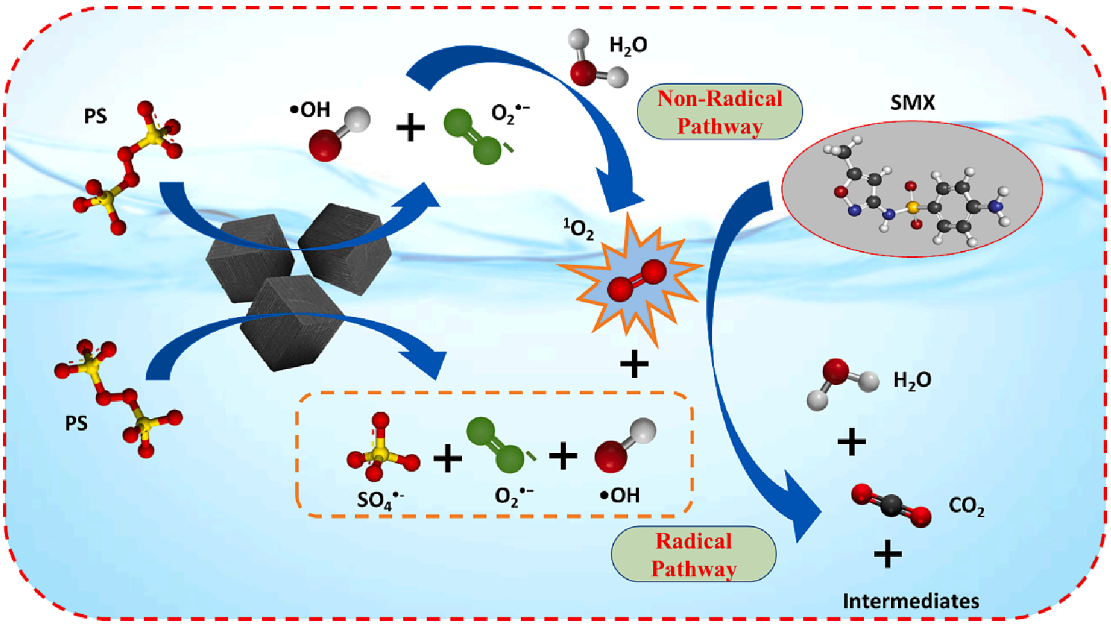

Fig. 8. A proposed SMX degradation mechanism.

strong triplet peaks of TEMP–$^1O_2$ were observed when TEMP was employed, indicating the presence of singlet oxygen ($^1O_2$). To further confirm the presence of $^1O_2$, NaN_3, a singlet oxygen quenching agent, was added to the reaction and the corresponding EPR spectrum was recorded. The reduced intensity of the triplet peaks of TEMP–$^1O_2$ indicated that the singlet oxygen was quenched, suggesting that the non-radical pathway was dominant in the NGC3/PS system.

To further verify the above argument, quenching tests were done to evaluate the active species as shown in Fig. 7**(c-f)** (Pseudo-first order reaction rate constants presented in **Figure S12**). Herein, methanol (MeOH) was employed to quench both $SO_4^{\bullet-}$ and •OH radicals while *tert*-butanol (tBA) was used to scavenge •OH radicals only. Further, p − benzoquinone (p − BQ) and sodium azide (NaN_3) were used to scavenge superoxide ($O_2^{\bullet-}$) and singlet oxygen respectively ($^1O_2$) [49]. Additionally, $AgNO_3$ was also employed to scavenge electrons (e^-) to identify the role of direct electron transfer [50]. SMX degradation efficiency was suppressed from 88% to 72% when MeOH was increased from 5 to 10 mM. In contrast, when tBA was varied from 5 to 10 mM, the SMX removal efficiency dropped from 81% to 67%. The above results suggested that both $SO_4^{\bullet-}$ and •OH radicals were present in the system, however, $SO_4^{\bullet-}$ played a minimal role compared to the •OH radicals. Further, when 5 and 10 mM of p − BQ were added to the NGC/PS system, the SMX oxidation efficiency dropped from 95% to 82% suggesting a partial role of $O_2^{\bullet-}$. To investigate the role of direct electron transfer as a non-radical pathway, $AgNO_3$ was used to quench electrons as depicted in **Figure S13**. The results showed a minimal role of direct electron transfer as SMX removal efficiency dropped to 92% and 86% upon adding 5 and 10 mM respectively [51]. Interestingly, SMX removal dropped from 72% to 58% when the NaN_3 amount was increased from 5 to 10 mM indicating that singlet oxygen played a crucial role in SMX degradation as was also confirmed by the EPR spectrum above. It was worth noting that SMX degradation by NGC3/PS system was led by both radical and non-radical mechanisms, with a dominance of non-radical species.

Based on the above discussions, a possible mechanism of SMX degradation can be developed as shown in Fig. 8. Firstly, PS was attached to the catalytic surface via chemical bonds and electron transfer leading to the formation of SO_4^{2-} (Eq. (1)). The activation of the PS by the NGC3 would then lead to the formation of $SO_4^{\bullet-}$ and $O_2^{\bullet-}$ (Eqs. (2) and (3)). The sulfate radical would further react with the hydroxide ions forming •OH (Eq. (4)). The as-formed hydroxyl radicals could further lead to the formation of $O_2^{\bullet-}$ via a series of addition and decomposition reactions (Eqs. (5)-(7)) [52,53]. Finally, the singlet oxygen could be generated by the recombination or disproportionation of •OH and $O_2^{\bullet-}$ (Eqs. (8)-(10)) [34,52,53]. In addition, the sulfate radicals could also react with $HO_2^{\bullet}$ to generate the singlet oxygen (Eq. (11)). Ultimately, the overall SMX degradation can be summarized in Eq. (12).

$$S_2O_8^{2-} + 2e^- \rightarrow 2SO_4^{2-} \quad (1)$$

$$S_2O_8^{2-} + 2H_2O \rightarrow HO_2^- + 2SO_4^{2-} + 3H^+ \quad (2)$$

$$S_2O_8^{2-} + HO_2^- \rightarrow SO_4^{\bullet-} + SO_4^{2-} + H^+ + O_2^{\bullet-} \quad (3)$$

$$SO_4^{\bullet-} + OH^- \rightarrow SO_4^{2-} + \bullet OH \quad (4)$$

$$\bullet OH + \bullet OH \rightarrow H_2O_2 \quad (5)$$

$$\bullet OH + H_2O_2 \rightarrow H_2O + HO_2^{\bullet} \quad (6)$$

$$HO_2^{\bullet} \rightarrow H^+ + O_2^{\bullet-} \quad (7)$$

$$\bullet OH + O_2^{\bullet-} \rightarrow {}^1O_2 + OH^- \quad (8)$$

$$O_2^{\bullet-} + 2H_2O \rightarrow H_2O_2 + 2OH^- + {}^1O_2 \quad (9)$$

$$HO_2^{\bullet} + O_2^{\bullet-} \rightarrow HO_2^- + {}^1O_2 \quad (10)$$

$$HO_2^{\bullet} + SO_4^{\bullet-} \rightarrow HSO_4^- + {}^1O_2 \quad (11)$$

$$NGC3 + PS \rightarrow SO_4^{\bullet-} / \bullet OH / O_2^{\bullet-} / {}^1O_2 + SMX \rightarrow \{....\text{Multiple steps}....\} \rightarrow CO_2 + H_2O + \text{by-products} \quad (12)$$

3.2.4. *Mineralisation of organic pollutants*

Fig. 9a shows the total organic carbon (TOC) tests used to analyse the mineralisation ability of the synthesised NGC3. The results show that approximately 68% of mineralisation ability is exhibited by NGC3. In comparison to the complete degradation of SMX, a lower TOC mineralisation ability would suggest that the SMX molecule would be broken to form a series of intermediates which would further be degraded rather than direct degradation of SMX to CO_2 and H_2O. To validate the above arguments, HPLC chromatograms (Fig. 9b) were analysed to identify any possible intermediates. The strong and sharp peak at t_R of 1.50 min

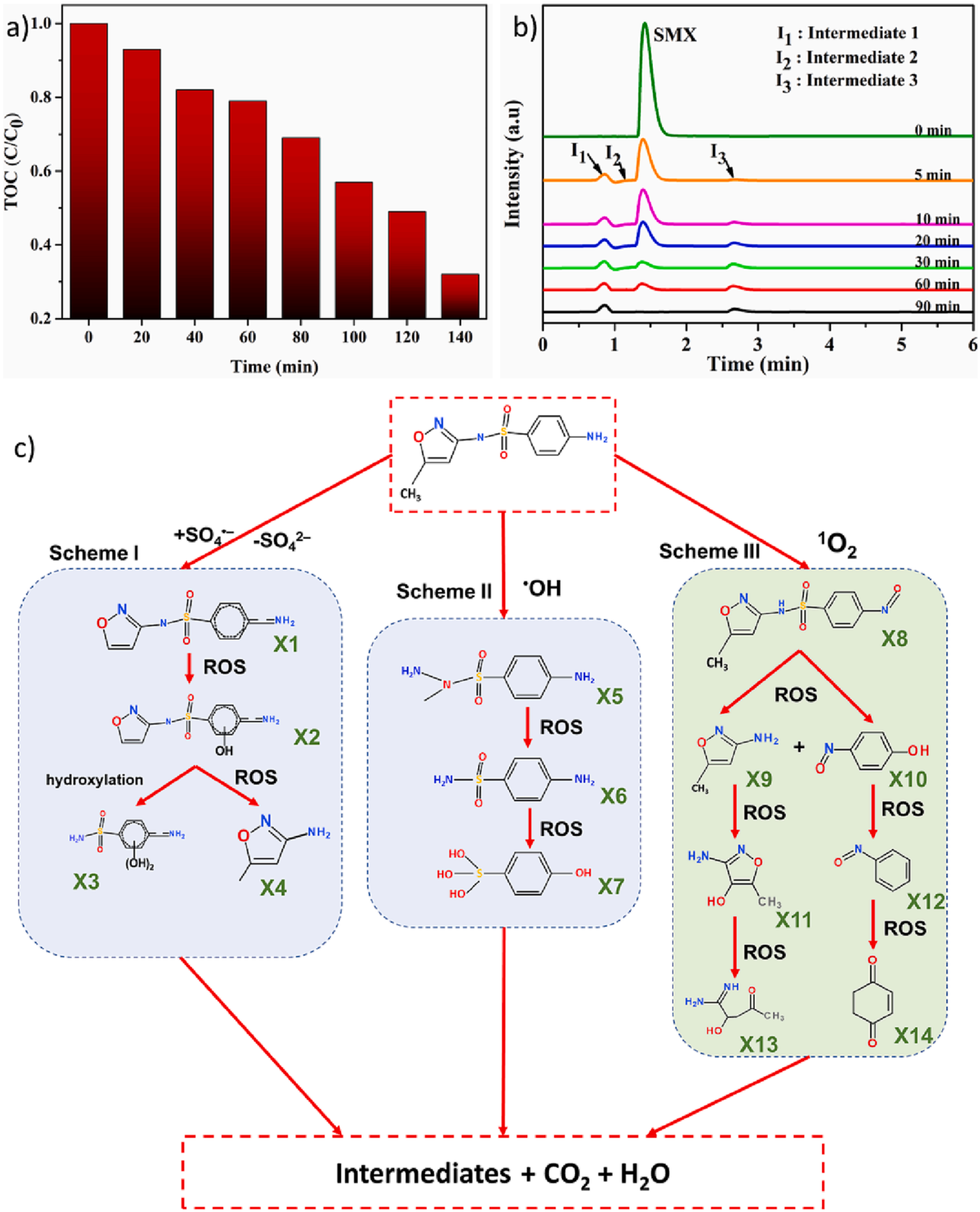

Fig. 9. (a) TOC analysis, (b) UHPLC spectra, and (c) proposed SMX degradation pathway. Reaction conditions: $[SMX]_0 = 20$ ppm, $[Catalyst]_0 = 0.2$ g/L, $[PS]_0 = 2.0$ g/L and T = 25 °C.

represents the SMX. After the addition of PS, three intermediates I_1, I_2 and I_3 can be seen at t_R of 0.80, 1.20 and 2.60 min respectively. It can be noted that the intermediate I_2 is mineralised after 60 min suggesting that it has a short lifetime and possible interconversion into relatively stable compounds [54,55].

As proposed earlier, the SMX degradation mechanism was facilitated by both radical and non-radical pathways. Following the vast literature review and the role of radical and non-radical pathways, three mineralisation pathways for SMX were proposed as shown in Fig. 9c. Schemes I and II shows radical-based pathways while scheme III depicts non-radical pathway. In scheme I, it is proposed that the sulfate radical would attack the SMX molecule resulting in the formation of a highly unstable radical cation SMX* (X1) which would be further hydrolyzed to SMX-OH (X2) [56]. As a result of the hydroxylation reaction of benzene ring, X2 could be split into X3 and X4 [57]. Further, the continuous attack on the X3 and X4 moieties could lead to ring opening and the formation of short chain acids (i.e., oxalic acid) which would then be mineralised to CO_2 and H_2O [58]. In scheme II, it is proposed that the hydroxyl radical would directly attack the SMX molecule resulting in isoxazole ring (X5) opening [59]. Thereafter, the continuous attack of ROS on X6 would cleavage the C − N bond resulting in the formation of X7 which would then be mineralised to aliphatic acid, CO_2, H_2O and SO_4^{2-} [34]. Scheme III shows the SMX mineralisation via non-radical mechanism. It is proposed that singlet oxygen would directly attack SMX molecules generating 4-nitrososulfamethoxazole (X8) [60]. Thereafter, the $^1O_2$ would attack X8 cleaving the S-N bond via hydroxylation forming X9 and X10 which could further be oxidised to X11 and X12 [34]. Afterwards, the oxidation of X11 would result in the formation of aliphatic hydrocarbon (X13) while further oxidation of X12 would form p-benzoquinone (X14) which was detected as I_1 in the HPLC chromatogram [23,34].

4. Conclusions

In conclusion, a number of doped and undoped GO macroscopic cubes were synthesised via a cross-linking and thermal annealing method and characterised by various techniques to investigate the physiochemical structure and properties. The prepared catalytic samples were introduced in PS assisted degradation of SMX. Degradation results showed that NGC3 had superior catalytic performance to GC, NGC1 and NGC5 with an activation energy of 16.74 kJ mol^{-1}. This study provided more insights into the nitrogen configuration in the sp^2 hybridised carbon network and its effect on catalysis. It was found that: (1) graphitic N and pyridinic N played a dominant role in the catalysis while pyrrolic N played a negligible role as confirmed by XPS analysis; (2) optimum nitrogen loading is important for the synthesis of efficient N-doped graphene-based catalysts as the N/C ratio played a vital role in the degradation efficiency explaining why NGC3 was a more efficient catalyst over NGC5 despite having a low N-loading compared to the latter; (3) the N/C ratio in N-doped graphene catalyst dominates the effect of specific surface area in the PS/NGC system for the degradation of SMX. Primary reaction parameters such as PS dosage, initial catalyst dosage, solution pH and reaction temperature were optimised to support the commercialisation. Further, stability and reusability tests showed that NGC3 had more than 77% degradation efficiency even after four cycles. The dominance of the non-radical pathway over the radical pathway was also proved following a series of quenching tests and EPR analysis. Finally, the SMX degradation pathway was proposed based on an extensive literature review and HPLC chromatography. This study could provide novel insights into the commercialisation of NGCs for wastewater remediation in near future based on their ability to overcome the shortcomings of powdered and metal-based catalysts.

CRediT authorship contribution statement

Rajan Arjan Kalyan Hirani: Conceptualization, Methodology, Investigation, Formal analysis, Writing – original draft. **Abdul Hannan Asif:** Formal analysis, Data curation. **Nasir Rafique:** Data curation. **Lei Shi:** Supervision, Resources, Validation. **Shu Zhang:** Supervision, Resources. **Martin Saunders:** Data curation. **Wenjie Tian:** Formal analysis, Data curation. **Shaobin Wang:** Supervision, Resources, Validation. **Hongqi Sun:** Supervision, Resources, Project administration, Writing – review & editing.

Declaration of Competing Interest

The authors declare that they have no known competing financial interests or personal relationships that could have appeared to influence the work reported in this paper.

Data availability

Data will be made available on request.

Acknowledgements

The author (Sun) would like to express his thanks for the support from the “Significant Research Achievement Award” from the Office of Deputy Vice-Chancellor Research, Edith Cowan University. The authors acknowledge the facilities and the scientific and technical assistance provided by A. Suvorova, H. Li and L. Kirilak of Microscopy Australia at the Centre for Microscopy, Characterisation & Analysis, The University of Western Australia, a facility funded by the University, State and Commonwealth Governments.

Appendix A. Supplementary data

Supplementary data to this article can be found online at https://doi.org/10.1016/j.seppur.2023.124110.

References

[1] K. Shang, R. Morent, N. Wang, Y. Wang, B. Peng, N. Jiang, N. Lu, J. Li, Degradation of sulfamethoxazole (SMX) by water falling film DBD Plasma/Persulfate: Reactive species identification and their role in SMX degradation, Chem. Eng. J. 431 (2022), 133916, https://doi.org/10.1016/j.cej.2021.133916.
[2] F. Ahmadijokani, H. Molavi, M. Rezakazemi, S. Tajahmadi, A. Bahi, F. Ko, T. M. Aminabhavi, J.-R. Li, M. Arjmand, UiO-66 metal–organic frameworks in water treatment: A critical review, Prog. Mater. Sci. 125 (2022), 100904, https://doi.org/10.1016/j.pmatsci.2021.100904.
[3] C.I. Ezugwu, J.M. Sonawane, R. Rosal, Redox-active metal-organic frameworks for the removal of contaminants of emerging concern, Sep. Purif. Technol. 284 (2022), 120246, https://doi.org/10.1016/j.seppur.2021.120246.
[4] Y. Minato, S. Dawadi, S.L. Kordus, A. Sivanandam, C.C. Aldrich, A.D. Baughn, Mutual potentiation drives synergy between trimethoprim and sulfamethoxazole, Nat. Commun. 9(1) (2018) 1003 10.1038/s41467-018-03447-x.
[5] J. Yan, J. Peng, L. Lai, F. Ji, Y. Zhang, B. Lai, Q. Chen, G. Yao, X. Chen, L. Song, Activation $CuFe_2O_4$ by Hydroxylamine for Oxidation of Antibiotic Sulfamethoxazole, Environ. Sci. Technol. 52 (24) (2018) 14302–14310, https://doi.org/10.1021/acs.est.8b03340.
[6] Y. Pan, Y. Zhang, M. Zhou, J. Cai, Y. Tian, Enhanced removal of antibiotics from secondary wastewater effluents by novel UV/pre-magnetized Fe0/H2O2 process, Water Res. 153 (2019) 144–159, https://doi.org/10.1016/j.watres.2018.12.063.
[7] Y. Liu, Q. Fan, J. Wang, Zn-Fe-CNTs catalytic in situ generation of H2O2 for Fenton-like degradation of sulfamethoxazole, J. Hazard. Mater. 342 (2018) 166–176, https://doi.org/10.1016/j.jhazmat.2017.08.016.
[8] J. Wang, R. Zhuan, Degradation of antibiotics by advanced oxidation processes: An overview, Sci. Total Environ. 701 (2020), 135023, https://doi.org/10.1016/j.scitotenv.2019.135023.
[9] X. Chen, W.-D. Oh, Z.-T. Hu, Y.-M. Sun, R.D. Webster, S.-Z. Li, T.-T. Lim, Enhancing sulfacetamide degradation by peroxymonosulfate activation with N-doped graphene produced through delicately-controlled nitrogen functionalization via tweaking thermal annealing processes, Appl. Catal. B: Environ. 225 (2018) 243–257, https://doi.org/10.1016/j.apcatb.2017.11.071.
[10] O. Vieira, R.S. Ribeiro, M. Pedrosa, A.R. Lado Ribeiro, A.M.T. Silva, Nitrogen-doped reduced graphene oxide – PVDF nanocomposite membrane for persulfate activation and degradation of water organic micropollutants, Chem. Eng. J. 402 (2020) 126117 10.1016/j.cej.2020.126117.
[11] C. Antolini, C.D. Spellman Jr., C.J. Otolski, G. Doumy, A.M. March, D.A. Walko, C. Liu, X. Zhang, B.T. Young, J.E. Goodwill, D. Hayes, Photochemical and

Photophysical Dynamics of the Aqueous Ferrate(VI) Ion, J. Am. Chem. Soc. 144 (49) (2022) 22514–22527, https://doi.org/10.1021/jacs.2c08048.
[12] P.V. Nidheesh, G. Divyapriya, F. Ezzahra Titchou, M. Hamdani, Treatment of textile wastewater by sulfate radical based advanced oxidation processes, Sep. Purif. Technol. 293 (2022) 121115 10.1016/j.seppur.2022.121115.
[13] D.B. Miklos, C. Remy, M. Jekel, K.G. Linden, J.E. Drewes, U. Hübner, Evaluation of advanced oxidation processes for water and wastewater treatment – A critical review, Water Res. 139 (2018) 118–131, https://doi.org/10.1016/j.watres.2018.03.042.
[14] B. Yang, H. Kang, Y.-J. Ko, H. Woo, G. Gim, J. Choi, J. Kim, K. Cho, E.-J. Kim, S.-G. Lee, H. Lee, J. Lee, Persulfate activation by nanodiamond-derived carbon onions: Effect of phase transformation of the inner diamond core on reaction kinetics and mechanisms, Appl. Catal. B: Environ. 293 (2021), 120205, https://doi.org/10.1016/j.apcatb.2021.120205.
[15] A. Shahzad, A. Jawad, J. Ifthikar, Z. Chen, Z. Chen, The hetero-assembly of reduced graphene oxide and hydroxide nanosheets as superlattice materials in PMS activation, Carbon 155 (2019) 740–755, https://doi.org/10.1016/j.carbon.2019.09.033.
[16] X. Cheng, H. Guo, Y. Zhang, G.V. Korshin, B. Yang, Insights into the mechanism of nonradical reactions of persulfate activated by carbon nanotubes: Activation performance and structure-function relationship, Water Res. 157 (2019) 406–414, https://doi.org/10.1016/j.watres.2019.03.096.
[17] R.A.K. Hirani, A.H. Asif, N. Rafique, L. Shi, S. Zhang, H. Wu, H. Sun, Wastewater Remediation Technologies Using Macroscopic Graphene-Based Materials: A Perspective, Front. Nanotechnol. 3 (2021), https://doi.org/10.3389/fnano.2021.688552.
[18] G.S.S. Mamaril, M.D.G. de Luna, K. Bindumadhavan, D.C. Ong, J.A.I. Pimentel, R.-A. Doong, Nitrogen and fluorine co-doped 3-dimensional reduced graphene oxide architectures as high-performance electrode material for capacitive deionization of copper ions, Sep. Purif. Technol. 272 (2021), 117559, https://doi.org/10.1016/j.seppur.2020.117559.
[19] L. Duan, X. Zhou, S. Liu, P. Shi, W. Yao, 3D-hierarchically structured Co_3O_4/graphene hydrogel for catalytic oxidation of Orange II solutions by activation of peroxymonosulfate, J. Taiwan Inst. Chem. Eng. 76 (2017) 101–108, https://doi.org/10.1016/j.jtice.2017.04.019.
[20] X. Duan, H. Sun, S. Wang, Metal-Free Carbocatalysis in Advanced Oxidation Reactions, Acc. Chem. Res. 51 (3) (2018) 678–687, https://doi.org/10.1021/acs.accounts.7b00535.
[21] W. Zhang, Y. Fu, J. Wang, X. Wang, 3D Hierarchically Porous Graphitic Carbon Nitride Modified Graphene-Pt Hybrid as Efficient Methanol Oxidation Catalysts, Adv. Mater. Interfaces 4(12) (2017) 1601219 10.1002/admi.201601219.
[22] C. Bao, S. Bi, H. Zhang, J. Zhao, P. Wang, C.Y. Yue, J. Yang, Graphene oxide beads for fast clean-up of hazardous chemicals, J. Mater. Chem. A 4 (24) (2016) 9437–9446, https://doi.org/10.1039/C6TA01411A.
[23] R.A.K. Hirani, A.H. Asif, N. Rafique, H. Wu, L. Shi, S. Zhang, X. Duan, S. Wang, M. Saunders, H. Sun, Three-dimensional nitrogen-doped graphene oxide beads for catalytic degradation of aqueous pollutants, Chem. Eng. J. 446 (2022), 137042, https://doi.org/10.1016/j.cej.2022.137042.
[24] F.M. Hassan, V. Chabot, J. Li, B.K. Kim, L. Ricardez-Sandoval, A. Yu, Pyrrolic-structure enriched nitrogen doped graphene for highly efficient next generation supercapacitors, J. Mater. Chem. A 1 (8) (2013) 2904–2912, https://doi.org/10.1039/C2TA01064J.
[25] N.R. Wilson, P.A. Pandey, R. Beanland, J.P. Rourke, U. Lupo, G. Rowlands, R.A. Römer, On the structure and topography of free-standing chemically modified graphene, New J. Phys. 12(12) (2010) 125010 10.1088/1367-2630/12/12/125010.
[26] D. Su, M. Cortie, G. Wang, Fabrication of N-doped Graphene–Carbon Nanotube Hybrids from Prussian Blue for Lithium–Sulfur Batteries, Adv. Energy Mater. 7(8) (2017) 1602014 10.1002/aenm.201602014.
[27] L. Qu, Y. Liu, J.-B. Baek, L. Dai, Nitrogen-Doped Graphene as Efficient Metal-Free Electrocatalyst for Oxygen Reduction in Fuel Cells, ACS Nano 4 (3) (2010) 1321–1326, https://doi.org/10.1021/nn901850u.
[28] S. Liu, H. Sun, A. Suvorova, S. Wang, One-pot hydrothermal synthesis of ZnO-reduced graphene oxide composites using Zn powders for enhanced photocatalysis, Chem. Eng. J. 229 (2013) 533–539, https://doi.org/10.1016/j.cej.2013.06.063.
[29] T. Wang, Z.-X. Chen, Y.-G. Chen, L.-J. Yang, X.-D. Yang, J.-Y. Ye, H.-P. Xia, Z.-Y. Zhou, S.-G. Sun, Identifying the Active Site of N-Doped Graphene for Oxygen Reduction by Selective Chemical Modification, ACS Energy Lett. 3 (4) (2018) 986–991, https://doi.org/10.1021/acsenergylett.8b00258.
[30] N.A. Elessawy, J. El Nady, W. Wazeer, A.B. Kashyout, Development of High-Performance Supercapacitor based on a Novel Controllable Green Synthesis for 3D Nitrogen Doped Graphene, Sci. Rep. 9(1) (2019) 1129 10.1038/s41598-018-37369-x.
[31] R.M.N.M. Rathnayake, H.W.M.A.C. Wijayasinghe, H.M.T.G.A. Pitawala, M. Yoshimura, H.-H. Huang, Synthesis of graphene oxide and reduced graphene oxide by needle platy natural vein graphite, Appl. Surf. Sci. 393 (2017) 309–315, https://doi.org/10.1016/j.apsusc.2016.10.008.
[32] Z. Lin, G. Waller, Y. Liu, M. Liu, C.-P. Wong, Facile Synthesis of Nitrogen-Doped Graphene via Pyrolysis of Graphene Oxide and Urea, and its Electrocatalytic Activity toward the Oxygen-Reduction Reaction, Adv. Energy Mater. 2 (7) (2012) 884–888, https://doi.org/10.1002/aenm.201200038.
[33] Y. Qu, J. Wang, Q. Ma, W. Shen, X. Pei, S. You, Q. Yin, X. Li, A novel environmental fate of graphene oxide: Biodegradation by a bacterium Labrys sp, WJW to support growth, Water Res. 143 (2018) 260–269, https://doi.org/10.1016/j.watres.2018.03.070.
[34] A.H. Asif, N. Rafique, R.A.K. Hirani, L. Shi, S. Zhang, S. Wang, H. Sun, Graphitic carbon nitride engineered α-Fe_2O_3/rGO heterostructure for visible-light-driven photochemical oxidation of sulfamethoxazole, Chem. Eng. J. 451 (2023), 138630, https://doi.org/10.1016/j.cej.2022.138630.
[35] C.H. Choi, M.W. Chung, H.C. Kwon, J.H. Chung, S.I. Woo, Nitrogen-doped graphene/carbon nanotube self-assembly for efficient oxygen reduction reaction in acid media, Appl. Catal. B: Environ. 144 (2014) 760–766, https://doi.org/10.1016/j.apcatb.2013.08.021.
[36] C. Zhang, L. Fu, N. Liu, M. Liu, Y. Wang, Z. Liu, Synthesis of Nitrogen-Doped Graphene Using Embedded Carbon and Nitrogen Sources, Adv. Mater. 23 (8) (2011) 1020–1024, https://doi.org/10.1002/adma.201004110.
[37] C. Wang, J. Kang, H. Sun, H.M. Ang, M.O. Tadé, S. Wang, One-pot synthesis of N-doped graphene for metal-free advanced oxidation processes, Carbon 102 (2016) 279–287, https://doi.org/10.1016/j.carbon.2016.02.048.
[38] S. Ye, G. Zeng, X. Tan, H. Wu, J. Liang, B. Song, N. Tang, P. Zhang, Y. Yang, Q. Chen, X. Li, Nitrogen-doped biochar fiber with graphitization from Boehmeria nivea for promoted peroxymonosulfate activation and non-radical degradation pathways with enhancing electron transfer, Appl. Catal. B: Environ. 269 (2020), 118850, https://doi.org/10.1016/j.apcatb.2020.118850.
[39] Y. Zhao, D. Wu, Y. Chen, Y. Li, X. Fan, F. Zhang, G. Zhang, W. Peng, Thermal removal of partial nitrogen atoms in N-doped graphene for enhanced catalytic oxidation, J. Colloid Interface Sci. 585 (2021) 640–648, https://doi.org/10.1016/j.jcis.2020.10.043.
[40] X. Duan, K. O'Donnell, H. Sun, Y. Wang, S. Wang, Sulfur and Nitrogen Co-Doped Graphene for Metal-Free Catalytic Oxidation Reactions, Small 11 (25) (2015) 3036–3044, https://doi.org/10.1002/smll.201403715.
[41] M. Feng, R. Qu, X. Zhang, P. Sun, Y. Sui, L. Wang, Z. Wang, Degradation of flumequine in aqueous solution by persulfate activated with common methods and polyhydroquinone-coated magnetite/multi-walled carbon nanotubes catalysts, Water Res. 85 (2015) 1–10, https://doi.org/10.1016/j.watres.2015.08.011.
[42] M. Nie, Y. Yang, Z. Zhang, C. Yan, X. Wang, H. Li, W. Dong, Degradation of chloramphenicol by thermally activated persulfate in aqueous solution, Chem. Eng. J. 246 (2014) 373–382, https://doi.org/10.1016/j.cej.2014.02.047.
[43] I. Othman, J. Hisham Zain, M. Abu Haija, F. Banat, Catalytic activation of peroxymonosulfate using $CeVO_4$ for phenol degradation: An insight into the reaction pathway, Appl. Catal. B: Environ. 266 (2020) 118601 10.1016/j.apcatb.2020.118601.
[44] Y. Li, H. Dong, L. Li, J. Xiao, S. Xiao, Z. Jin, Efficient degradation of sulfamethazine via activation of percarbonate by chalcopyrite, Water Res. 202 (2021), 117451, https://doi.org/10.1016/j.watres.2021.117451.
[45] J. Wang, S. Wang, Effect of inorganic anions on the performance of advanced oxidation processes for degradation of organic contaminants, Chem. Eng. J. 411 (2021), 128392, https://doi.org/10.1016/j.cej.2020.128392.
[46] S. Chen, M. Cai, Y. Liu, L. Zhang, L. Feng, Effects of water matrices on the degradation of naproxen by reactive radicals in the UV/peracetic acid process, Water Res. 150 (2019) 153–161, https://doi.org/10.1016/j.watres.2018.11.044.
[47] S. Ye, W. Xiong, J. Liang, H. Yang, H. Wu, C. Zhou, L. Du, J. Guo, W. Wang, L. Xiang, G. Zeng, X. Tan, Refined regulation and nitrogen doping of biochar derived from ramie fiber by deep eutectic solvents (DESs) for catalytic persulfate activation toward non-radical organics degradation and disinfection, J. Colloid Interface Sci. 601 (2021) 544–555, https://doi.org/10.1016/j.jcis.2021.05.080.
[48] R. Luo, M. Li, C. Wang, M. Zhang, M.A. Nasir Khan, X. Sun, J. Shen, W. Han, L. Wang, J. Li, Singlet oxygen-dominated non-radical oxidation process for efficient degradation of bisphenol A under high salinity condition, Water Res. 148 (2019) 416–424, https://doi.org/10.1016/j.watres.2018.10.087.
[49] A.B. Azzam, A.O. Abd El-Aziz, S.K. Mohamed, Activation of persulfate using CuS synthesized by ultrafast solid-state reaction for removal of organic pollutants from wastewater: Economical synthesis, catalytic performance, and mechanism, Sep. Purif. Technol. 284 (2022) 120238 10.1016/j.seppur.2021.120238.
[50] G. Nie, L. Xiao, J. Bi, S. Wang, X. Duan, New insight to piezocatalytic peroxymonosulfate activation: The critical role of dissolved oxygen in mediating radical and nonradical pathways, Appl. Catal. B: Environ. 315 (2022), 121584, https://doi.org/10.1016/j.apcatb.2022.121584.
[51] A.H. Asif, N. Rafique, R.A.K. Hirani, H. Wu, L. Shi, S. Zhang, S. Wang, Y. Yin, M. Saunders, H. Sun, Morphology/facet-dependent photo-Fenton-like degradation of pharmaceuticals and personal care products over hematite nanocrystals, Chem. Eng. J. 432 (2022), 134429, https://doi.org/10.1016/j.cej.2021.134429.
[52] Y. Qi, B. Ge, Y. Zhang, B. Jiang, C. Wang, M. Akram, X. Xu, Three-dimensional porous graphene-like biochar derived from Enteromorpha as a persulfate activator for sulfamethoxazole degradation: Role of graphitic N and radicals transformation, J. Hazard. Mater. 399 (2020), 123039, https://doi.org/10.1016/j.jhazmat.2020.123039.
[53] X. Long, Z. Xiong, R. Huang, Y. Yu, P. Zhou, H. Zhang, G. Yao, B. Lai, Sustainable Fe(III)/Fe(II) cycles triggered by co-catalyst of weak electrical current in Fe(III)/peroxymonosulfate system: Collaboration of radical and non-radical mechanisms, Appl. Catal. B: Environ. 317 (2022), 121716, https://doi.org/10.1016/j.apcatb.2022.121716.
[54] S. Wang, Y. Liu, J. Wang, Iron and sulfur co-doped graphite carbon nitride (FeOy/S-g-C_3N_4) for activating peroxymonosulfate to enhance sulfamethoxazole degradation, Chem. Eng. J. 382 (2020), 122836, https://doi.org/10.1016/j.cej.2019.122836.
[55] Z. He, H. Wang, M. Li, L. Feng, J. Niu, Z. Li, X. Jia, G. Hu, Amorphous cobalt oxide decorated halloysite nanotubes for efficient sulfamethoxazole degradation activated by peroxymonosulfate, J. Colloid Interface Sci. 607 (2022) 857–868, https://doi.org/10.1016/j.jcis.2021.08.168.

[56] Y. Ji, Y. Fan, K. Liu, D. Kong, J. Lu, Thermo activated persulfate oxidation of antibiotic sulfamethoxazole and structurally related compounds, Water Res. 87 (2015) 1–9, https://doi.org/10.1016/j.watres.2015.09.005.
[57] Y. Yu, Y. Ji, J. Lu, X. Yin, Q. Zhou, Degradation of sulfamethoxazole by Co_3O_4-palygorskite composites activated peroxymonosulfate oxidation, Chem. Eng. J. 406 (2021), 126759, https://doi.org/10.1016/j.cej.2020.126759.
[58] P. Yan, Q. Sui, S. Lyu, H. Hao, H.F. Schröder, W. Gebhardt, Elucidation of the oxidation mechanisms and pathways of sulfamethoxazole degradation under Fe(II) activated percarbonate treatment, Sci. Total Environ. 640–641 (2018) 973–980, https://doi.org/10.1016/j.scitotenv.2018.05.315.
[59] F. Liu, Y. Zhang, S. Wang, T. Gong, M. Hua, J. Qian, B. Pan, Metal-free biomass with abundant carbonyl groups as efficient catalyst for the activation of peroxymonosulfate and degradation of sulfamethoxazole, Chem. Eng. J. 430 (2022), 132767, https://doi.org/10.1016/j.cej.2021.132767.
[60] Y. Zhou, J. Jiang, Y. Gao, S.-Y. Pang, Y. Yang, J. Ma, J. Gu, J. Li, Z. Wang, L.-H. Wang, L.-P. Yuan, Y. Yang, Activation of peroxymonosulfate by phenols: Important role of quinone intermediates and involvement of singlet oxygen, Water Res. 125 (2017) 209–218, https://doi.org/10.1016/j.watres.2017.08.049.